Effect of Rotor Blade Elasticity on UAM Quadrotor Acoustics

Sesi Kottapalli *
Aeromechanics Office
NASA Ames Research Center
Moffett Field, CA, USA

Christopher Silva
Aeromechanics Office
NASA Ames Research Center
Moffett Field, CA, USA

D. Douglas Boyd, Jr.
Aeroacoustics Branch
NASA Langley Research Center
Hampton, VA, USA

ABSTRACT

The 6-passenger quadrotor concept vehicle designed under the NASA Revolutionary Vertical Lift Technology (RVLT) Project is considered for acoustic analysis. The tip speed is 550 ft/sec, with three blades per rotor (550/3). Originally, the blades were rigid, uniform spanwise, and with flap and pitch degrees of freedom. The blade model has since been updated: a lag hinge was added, and nonuniformities and elastic properties were introduced. Four blade models are considered: 1) original model, rigid uniform flap-pitch; 2) rigid uniform flap-lag-pitch; 3) rigid nonuniform flap-lag-pitch; and 4) elastic nonuniform flap-lag-torsion. Predictions are made for three flight conditions (approach, flyover, and takeoff) using the four blade models. The RVLT Toolchain is exercised using CAMRAD II and pyaaron/AARON/ANOPP2. Quadrotor trim and performance, 0.75R vertical blade loading for all four rotors, and noise sources are analyzed. Also, the contributions of the front and rear rotor pairs to noise are studied. In approach and flyover, a 2 dBA loading noise difference (delta) is predicted between blade models 1 and 4 (delta for takeoff is smaller, 1 dBA). Most of this noise delta is due to the lag hinge and nonuniformities, which is consistent with the results of a 2022 study that had considered only the approach condition; the current results extend this conclusion to flyover and takeoff also. The insensitivity of quadrotor noise to blade elasticity is currently attributed to the high blade torsional stiffness (frequency 6.41 per rev) and the small blade radius (9 ft) of the 550/3 design. Suggestions for potential follow-on work are given.

NOTATION

550/3	quadrotor concept vehicle with tip speed=550 ft/sec and 3 blades per rotor
AARON	ANOPP2's Aeroacoustic ROtor Noise tool
ANOPP2	Aircraft Noise Prediction Program - Second Generation
bb	broadband (self) noise
Blade model 1	rigid uniform flap-pitch
Blade model 2	rigid uniform flap-lag-pitch
Blade model 3	rigid nonuniform flap-lag-pitch
Blade model 4	elastic nonuniform flap-lag-torsion
BVI	blade vortex interaction
CAMRAD II	Comprehensive Analytical Model of Rotorcraft Aerodynamics and Dynamics
EPNL	Effective Perceived Noise Level, EPNdB
FLP	flap-lag-pitch
FLT	flap-lag-torsion
FP	flap-pitch
Lmax	maximum noise level, A-weighted, dBA
loadz	blade Z direction (vertical) load in airframe axes, + down, N/m. (-loadz) + up
NDARC	NASA Design and Analysis of Rotorcraft
nonunif	nonuniform inertial and stiffness properties
OASPL	Overall Sound Pressure Level, dBA
pyaaron	Python tool to aid running AARON
RCOTools	RotorCraft Optimization Tools
t+l	thickness plus loading noise
UAM	Urban Air Mobility
unif	uniform inertial and stiffness properties

**Corresponding author. Presented at the Vertical Flight Society (VFS) 79th Annual Forum & Technology Display, May 16-18, 2023, West Palm, Florida, USA.*

INTRODUCTION

Recently, Ref. 1 considered the practical conceptual design of quieter urban VTOL aircraft. Several concept vehicles were studied in Ref. 1, including a 6-passenger quadrotor, Figs. 1a-1b. For this quadrotor, Ref. 2 used the RVLT Toolchain (Ref. 3, referred to hereafter as the "toolchain") to identify and analyze the noise sources, with the goal of providing guidance toward best practices for an application of the toolchain.

The research reported in this paper is a follow-on study to Ref. 2 which had mainly considered rigid blades. Preliminary results for an elastic blade were also presented in Ref. 2 for only the approach flight condition. In the current study, noise is predicted for three flight conditions: approach, flyover, and takeoff. Noise is calculated and analyzed for the quadrotor concept vehicle with elastic blades using the toolchain. The concept vehicle has a tip speed of 550 ft/sec, with three blades per rotor (550/3). The blade radius is ~9 ft and the design RPM is ~584. Specifics of the three flight conditions were determined by FAA certification standards (Ref. 1) and obtained from NDARC (Ref. 4). The three flight speeds are as follows: approach ~50 kts, flyover ~120 kts, and takeoff ~55 kts.

Trends of the individual rotor noise sources – thickness, loading, and self (broadband) – are studied. Noise comparison is done at the FAA centerline observer location using the A-weighted Lmax and the duration-based

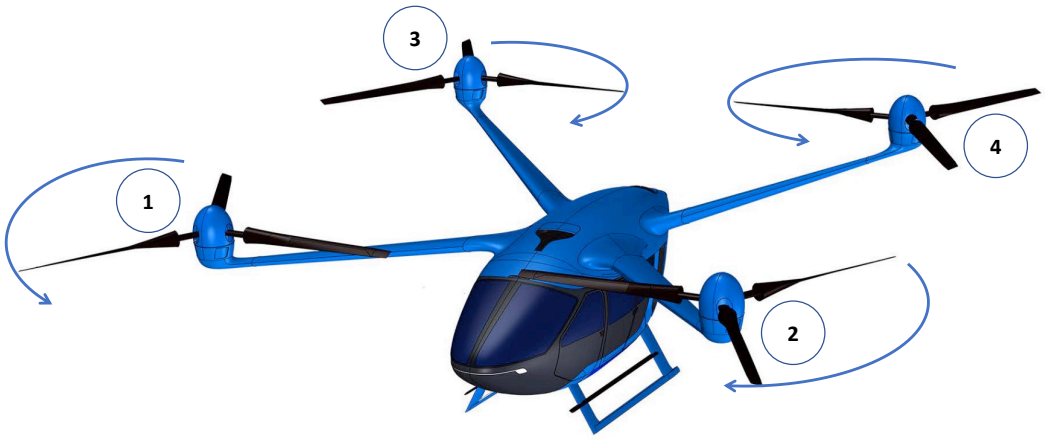

Figure 1a. Quadrotor isometric view, marked with rotor rotation direction and numbering, Ref. 1.

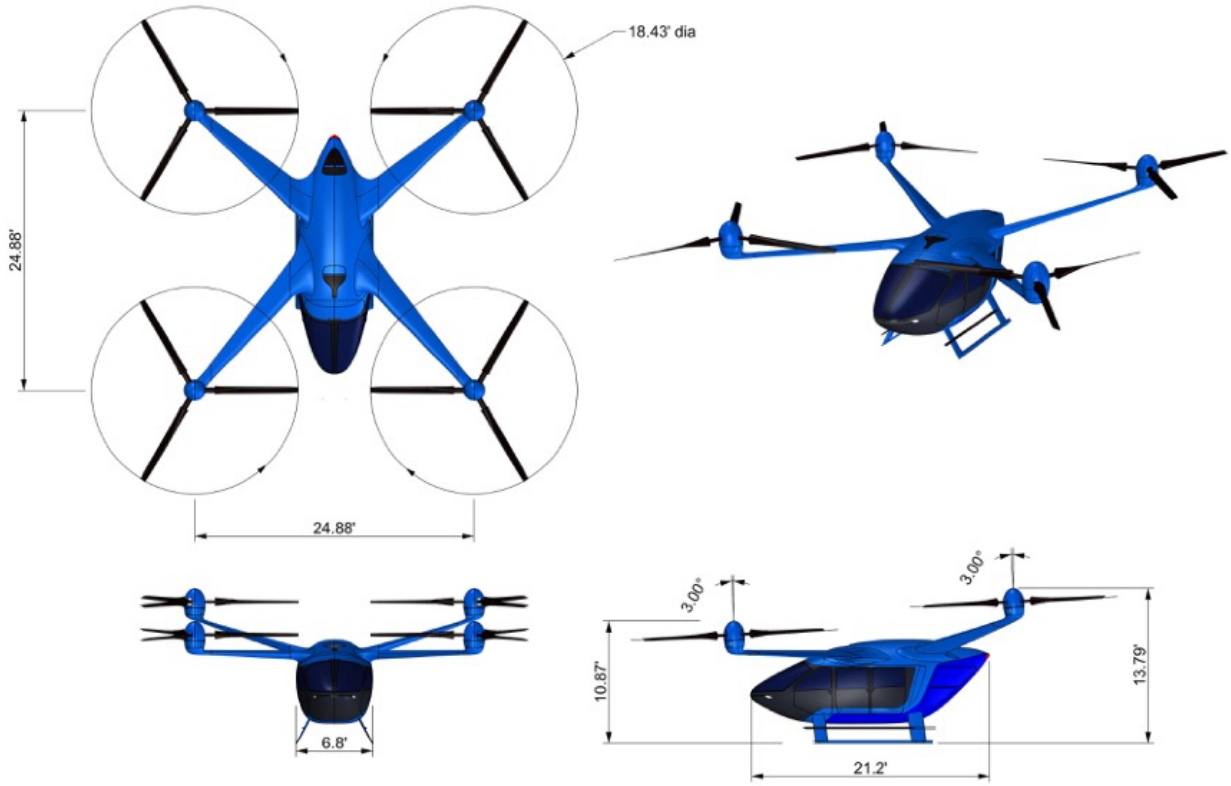

Figure 1b Quadrotor technical drawings, Ref. 1.

effective perceived noise level (EPNL). Results include quadrotor trim and power quantities, vertical blade loading for all four rotors, quadrotor noise predictions, and the contributions of the front and rear rotor pairs to noise.

As background, for conventional rotorcraft, Refs. 5-9 have included rotor blade elasticity in their noise calculations. Blade flexibility is usually accounted for by including elastic bending and torsional deformations. Of the above references, Ref. 5 is unique in that it additionally considers changes in the blade surface area due to surface deformation. Reference 6 brings out the importance of blade torsional stiffness in the prediction of BVI noise. Reference 7 concludes that "blade dynamics and flexibility must be properly incorporated in any acoustic simulation." Reference 8 notes the importance of blade-vortex miss distance, which can strongly affect BVI noise: "The miss distance is strongly influenced by tip trajectory and blade elastic deformation. The miss distance depends on … blade tip deflections at the blade-vortex formation as well as the interaction...". Reference 9 notes that "The numerical results indicate that inclusion of the MR [main rotor] elastic blade deformation in the simulation has clearly improved the correlation against the measured data…". The current study analyzes the acoustics of the NASA 6-passenger quadrotor concept vehicle with elastic rotor blades. This study examines the importance of blade elasticity for this non-conventional rotorcraft with multiple rotors. Initial results (approach only) presented in Ref. 2 indicated a lack of sensitivity of quadrotor noise to blade elasticity. The current study additionally considers flyover and takeoff.

RVLT TOOLCHAIN

The NASA Revolutionary Vertical Lift Technology (RVLT) Project has been developing tools to predict rotorcraft attributes for more than a decade (Ref. 3). In aeromechanics and rotorcraft design, these attributes include noise, performance, handling qualities, vibration, and cost. RVLT has also been developing various software packages to link individual, discipline-based prediction tools and create a unified toolchain. As a result, today, the toolchain covers a broad range of disciplines. In addition to the tools themselves, NASA is seeking to document best practices for using the tools and provide validation data, such that the toolchain is quantitatively meaningful and may be reliably exercised by conceptual design engineers in the U.S. government, industry, and academia.

Historically, disparate pieces of software, each performing a portion of the VTOL aircraft design and analysis task, have been developed, validated, and employed. These tools have been tailored to subsets of the design problem and developed by domain experts for their own use. As a result, little effort had been expended in ensuring interoperability with other codes, nor with providing ease-of-use for novice or non-expert users.

In place of the loosely organized collection of disparate software, a distinct "toolchain" of VTOL aircraft design and analysis tools is necessary for efficient and successful development of these vehicles. The RVLT Project is actively improving the usability and interoperability of the software elements, producing documentation, gathering validation data, and providing test cases, to produce an integrated toolchain.

Figure 2 outlines the currently relevant part of the toolchain. The rotorcraft comprehensive analysis CAMRAD II (Ref. 10) is used. CAMRAD II provides azimuthal variations of the lifting-line blade loadings (forces) and motions to the acoustic tools. These mostly "dynamics" related quantities are provided by the CAMRAD II "sound sensor." Blade sound sensors provide the information needed to calculate aerodynamically generated sound of the rotor using a compact loading formulation that is consistent with the lifting-line aerodynamic model. Thickness noise is computed using geometry provided by the sound sensor along with user input of the spanwise distribution of blade maximum thickness. There is a sensor for each aerodynamic collocation point (quarter chord, at the midpoint of the spanwise aerodynamic panel). All quantities are in the airframe reference frame. A set of Python libraries that serve as application interfaces/wrappers for the execution of CAMRAD II is also a part of the toolchain (RCOTools, RotorCraft Optimization Tools, Ref. 11). RCOTools is not shown in Fig. 2.

"pyaaron," a Python-based wrapper script, provides an interface for application-specific user inputs. pyaaron also extracts sound sensor data that are then passed on to the acoustic tools. The acoustic calculations are performed using the following tools: ANOPP2 (Aircraft NOise Prediction Program 2) and AARON (ANOPP2's Aeroacoustic ROtor Noise tool), Ref. 12. In this context, AARON is an ANOPP2 software tool written in Fortran that runs the ANOPP2 Farassat Formulation 1A Function Model (AFFIFM) for tone noise and/or ANOPP2's Self Noise Internal Function Module (ASNIFM) for rotor broadband self noise.

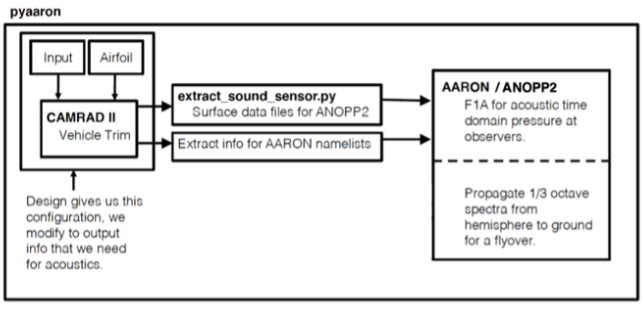

Figure 2. CAMRAD II plus AARON/ANOPP2 with pyaaron as the wrapper script.

QUADROTOR MODELING

Figure 1a shows the rotor rotation direction and rotor numbering scheme. The right-front and left-rear rotors (rotors

1 and 4, respectively) turn counterclockwise, and the left-front and right-rear rotors (rotors 2 and 3, respectively) turn clockwise. The CAMRAD II model of the quadrotor is summarized as follows: four rotors, rigid or elastic blades, collective control, constant RPM, rolled-up free wake (single tip vortex), and 6-DOF trim (zero average net forces and moments). The basic rigid blades have uniform (constant) spanwise inertial and stiffness properties; the blade root includes non-coincident flap hinge and pitch bearing (FP). For the elastic blades a fully articulated model is considered – a lag hinge is also included, in addition to the flap hinge and the pitch bearing. Thus, the elastic blade analysis is performed for an articulated blade with flap, lag, and torsion degrees of freedom (FLT). All blade models have linear taper (tip chord/root chord=0.75) and linear twist (-12 deg). The 550/3 elastic anisotropic blades were designed for this paper. The spanwise and cross-sectional properties were obtained using IXGEN/VABS (Refs. 13-14). The elastic blades have nonuniform inertial and stiffness properties. Aerodynamically, fully-coupled rotor wakes were evaluated. This setting is likely to be the most accurate depiction of the phenomena, as it can capture potentially important interactions due to strong vortices from not only the other blades on the same rotor, but also from blades of another rotor (rotor-rotor interaction). The quadrotor design has already included a mitigation of rotor-rotor interaction in forward flight by elevating the rear rotors relative to the front rotors, Fig. 1b (Ref. 1).

The noise tool AARON calculates the 1/3 octave spectrum at each point of a 19x19 hemisphere underneath the vehicle. This calculation is based on the CAMRAD II outputs and a small amount of supplemental information and includes both tonal sources (thickness and loading noise) and broadband noise (trailing edge self noise), Ref. 1.

RESULTS

To ensure that the effect of blade elasticity on quadrotor noise is studied in a consistent manner, the following four analytical blade models are considered, and the corresponding noise results compared. In this paper, "uniform" refers to uniform (constant) spanwise inertial and stiffness properties and "nonuniform" refers to inertial and stiffness properties that vary with span. In increasing complexity, the blade models are:

1. Rigid blade with uniform spanwise properties, with flap hinge and pitch bearing (*rgd unif FP*). This blade model was used in Ref. 2 (and the quadrotor-related predictions of Ref. 1). This is the original blade model.
2. Rigid blade with uniform spanwise properties, with flap and lag hinges and pitch bearing (*rgd unif FLP*).
3. Rigid blade with nonuniform spanwise properties, with flap and lag hinges and pitch bearing (*rgd nonunif FLP*). This is a rigid beam version of the elastic blade in item 4.
4. Elastic anisotropic blade with nonuniform spanwise and cross-sectional properties, with flap and lag hinges and pitch bearing (*elastic nonunif FLT*). The natural frequencies of the blade are given in Table 1.

Table 1. Blade frequencies, 550/3.

Mode	Frequency, per rev
1st lag	0.27
1st flap	1.03
2nd flap	2.91
Torsion	6.41
2nd lag	7.69
3rd flap	11.38

Noise predictions for three flight conditions (approach, flyover, and takeoff) and four blade models are obtained for the 550/3 concept vehicle (tip speed is 550 ft/sec, with three blades per rotor). The blade radius is ~9 ft and the design RPM is ~584. Specifics of the three flight conditions were determined by FAA certification standards in the same manner as in Ref. 1. The three flight speeds are as follows: approach ~50 kts, flyover ~120 kts, and takeoff ~55 kts.

Results are presented separately for each flight condition and include the following:

- Quadrotor trim and performance quantities
- Vertical blade loading loadz at 0.75R. loadz is in the airframe frame
- Quadrotor noise predictions.

A separate section contains summary results for all three flight conditions. Lastly, the contributions of the front and rear rotor pairs to noise are shown.

Approach

Quadrotor trim and performance, approach. Results for approach (6-deg descent, ~50 kts) are shown in Figs. 3a-3h for the four blade models. The trim and performance quantities shown include the blade collective, quadrotor pitch, rotor thrust and power. Figures 3a-3b show the average collective and quadrotor pitch angle required for trim. The effect of rotor-rotor interference can be seen in Figs. 3c-3d: the rear rotors (# 3 and 4, Fig. 1a) require increased collective while producing a smaller amount of thrust compared to the front rotors (# 1 and 2, Fig. 1a). Consistent with Figs. 3c-3d, Figs. 3e-3f show that the rear rotors (# 3 and 4) consume more power compared to the front rotors (# 1 and 2). The induced and profile powers are shown in Figs. 3g-3h. The propulsive and climb powers are not shown.

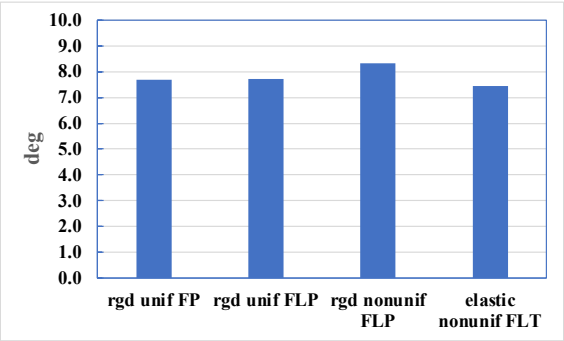

Figure 3a. Collective, average, approach.

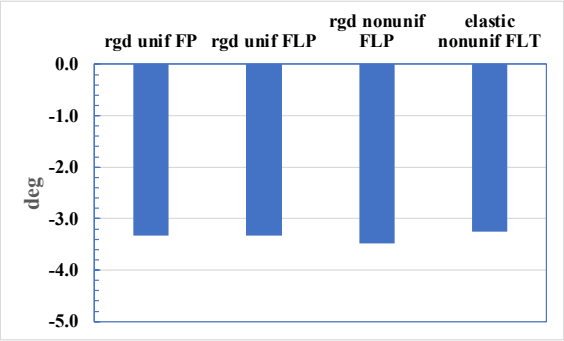

Figure 3b. Quadrotor pitch, approach.

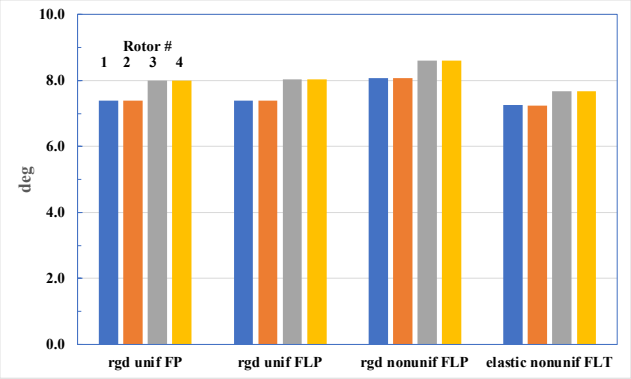

Figure 3c. Collective, rotors 1-4, approach.

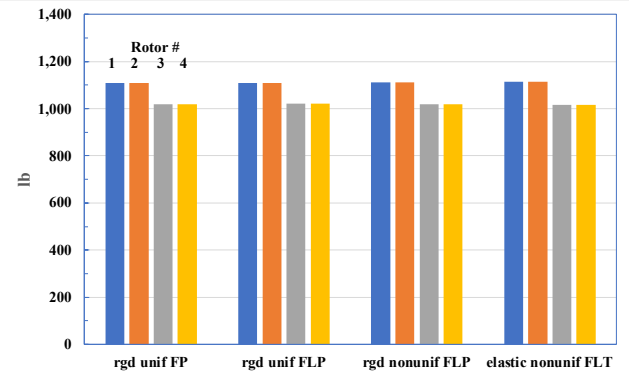

Figure 3d. Thrust, rotors 1-4, approach.

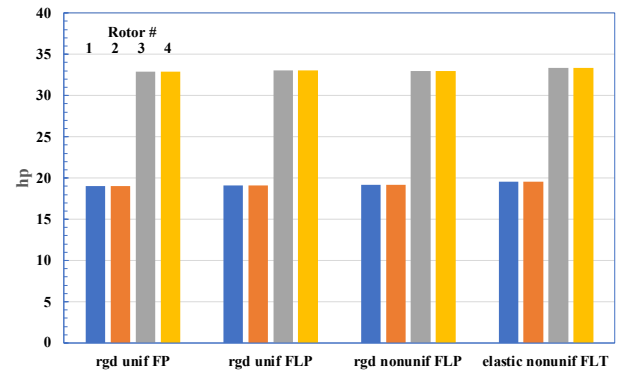

Figure 3e. Total power, approach.

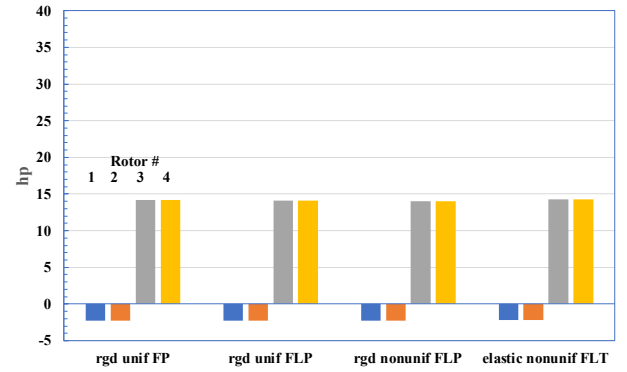

Figure 3f. Interference power, approach.

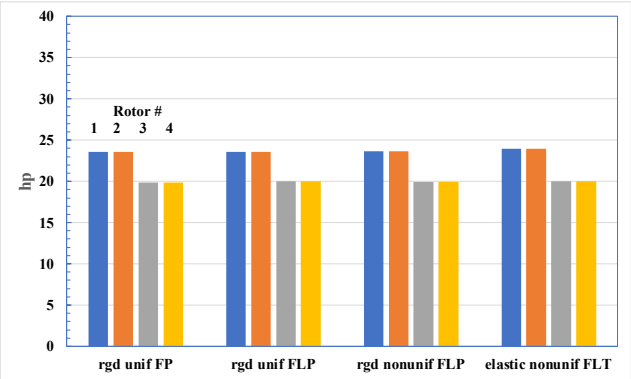

Figure 3g. Induced power, approach.

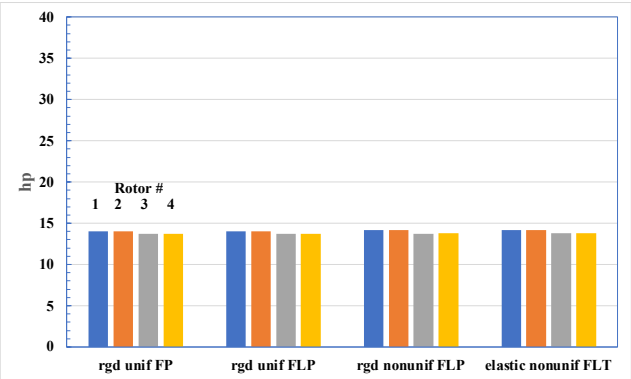

Figure 3h. Profile power, approach.

Vertical blade loading, approach. Figure 4 shows the vertical 0.75R blade loading (loadz) for all four rotors for blade model 1. There is longitudinal symmetry – the front left and right rotors behave in almost the same manner; the same holds for the rear rotor pair. In the following figures, results for only the right-side rotor pair (front and rear right) are shown. Figures 5a-5c show comparisons of loadz for the four blade models; two blade models are considered in each figure. Figure 5a shows loadz for blade models 1 and 2, Fig. 5b for models 2 and 3, and Fig. 5c for blade models 3 and 4. Lastly, Fig. 6 shows loadz for blade models 1 and 4. Reference 2 showed the rigid blade prediction for the front right rotor (Fig. 4d, Ref. 2), which is the same as the blue dashed-dotted line in Fig. 6. Figures 5c and 6 show that blade elasticity has a significant effect on the vertical blade loading. Interestingly, Fig. 6 shows that the effect of blade elasticity on vertical blade loading is primarily between 120 and 270 deg. Also, Figs. 4-6 show that the mean loading is greater for the front rotors, consistent with Fig. 3d.

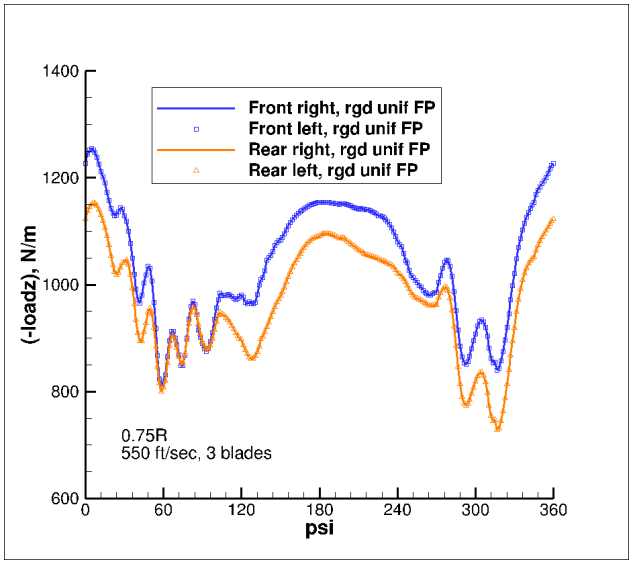

Figure 4. 0.75R, rigid uniform FP (blade model 1), all four rotors, approach.

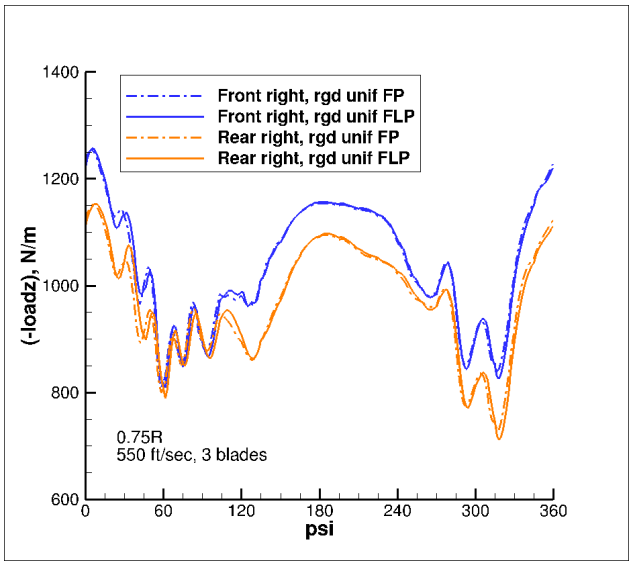

Figure 5a. 0.75R, rigid uniform FP and FLP (blade models 1 and 2), approach.

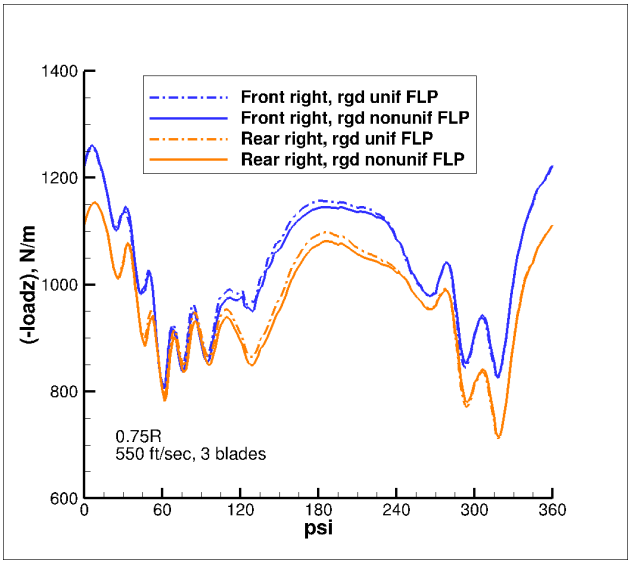

Figure 5b. 0.75R, rigid uniform and nonuniform FLP (blade models 2 and 3), approach.

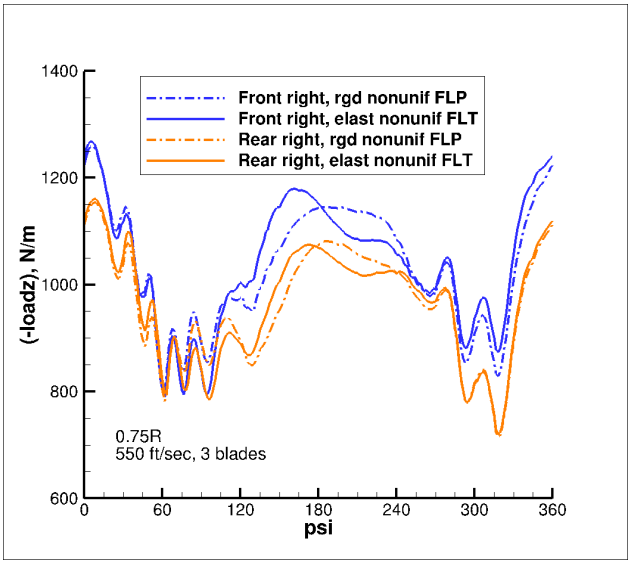

Figure 5c. 0.75R, rigid nonuniform FLP and elastic nonuniform FLT (blade models 3 and 4), approach.

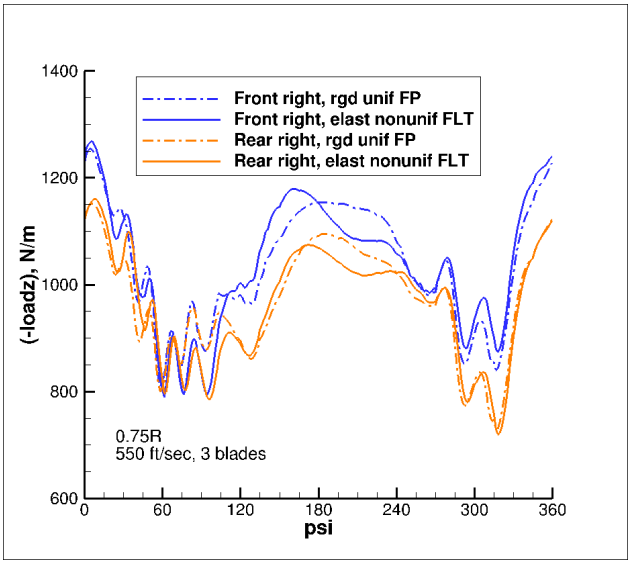

Figure 6. 0.75R, rigid uniform FP and elastic nonuniform FLT (blade models 1 and 4), approach.

Quadrotor noise, approach. Table 2 (placed after the last section of the paper) shows predicted A-weighted Lmax and EPNL for the four blade models; Fig. 7 shows the same information as a column chart. The following observations can be made (basically, these are the same as Conclusion 4 of Ref. 2):

a) For all four blade models, only the loading noise is different – the thickness and broadband noise are almost the same for all four models. Thus, the trend for the total noise follows the trend for the loading noise.

b) The addition of the lag hinge to the rigid blade with uniform properties reduces the loading noise by ~1.5 dBA (blade models 1 and 2).

c) For the rigid nonuniform blade, a further ~1 dBA reduction in loading noise is obtained (blade models 2 and 3).

d) Results for blade models 3 and 4 do not show any significant difference in the loading noise levels (69 dBA). Pending further study, preliminary reasons for this insensitivity to elasticity are:

- The high torsional stiffness of the blade (torsion frequency is 6.41 per rev)
- The small radius of the blade. Compared to conventional helicopter blades, 550/3 has shorter blades (conventional blades have a radius 2 to 3 times larger than the 9 ft radius of the quadrotor).

This result needs to be confirmed through further analysis with current and other blade designs and additional operating conditions.

e) Even though the total (and loading) A-weighted Lmax noise levels show sensitivity to the current blade models, EPNL is roughly the same for all blade models.

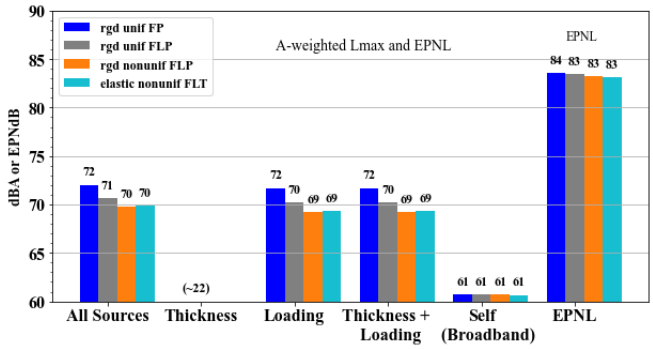

Figure 7. Quadrotor noise sources (all four rotors), blade models 1-4, approach.

Flyover

Quadrotor trim and performance, flyover. Results for flyover (~120 kts) are shown in Figs. 8a-8h. Figure 8f shows that the interference power in flyover is very small, which is unlike that in approach.

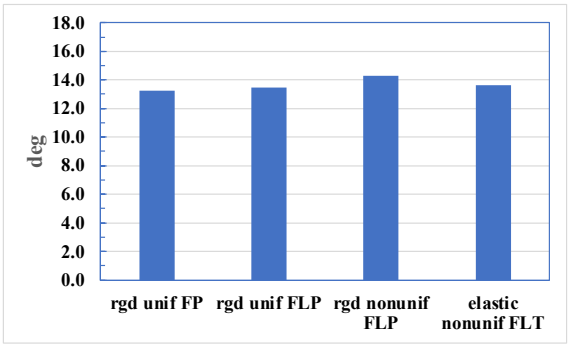

Figure 8a. Collective, average, flyover.

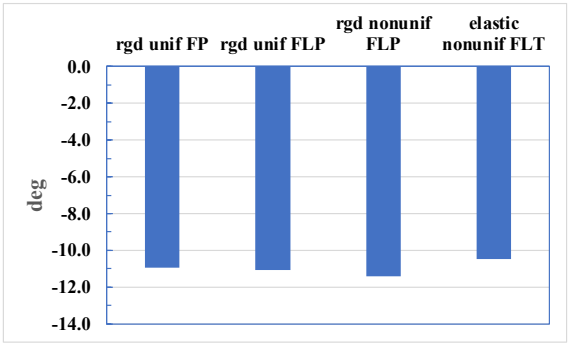

Figure 8b. Quadrotor pitch, flyover.

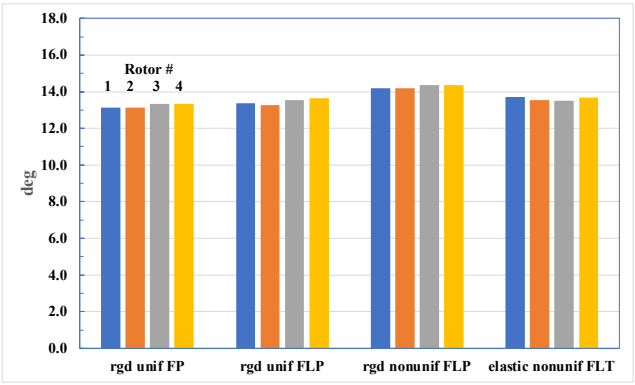

Figure 8c. Collective, rotors 1-4, flyover.

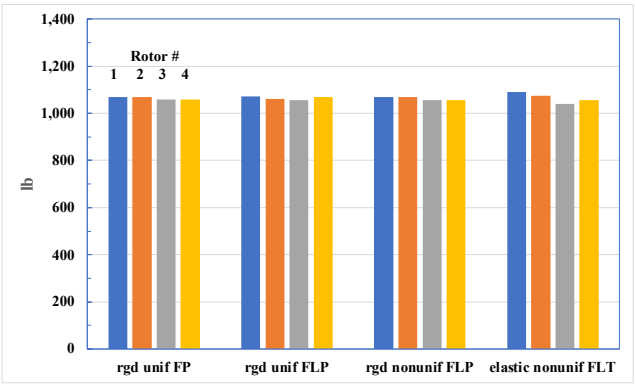

Figure 8d. Thrust, rotors 1-4, flyover.

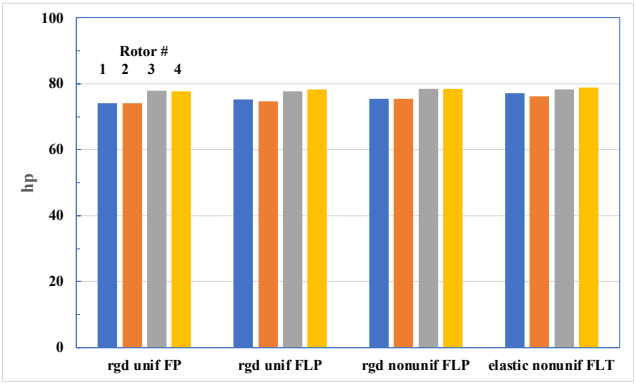

Figure 8e. Total power, flyover.

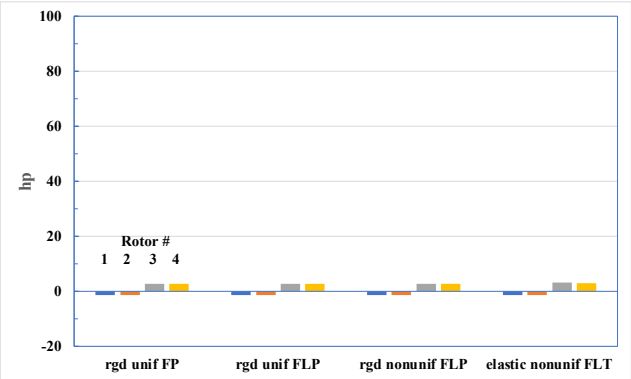

Figure 8f. Interference power, flyover.

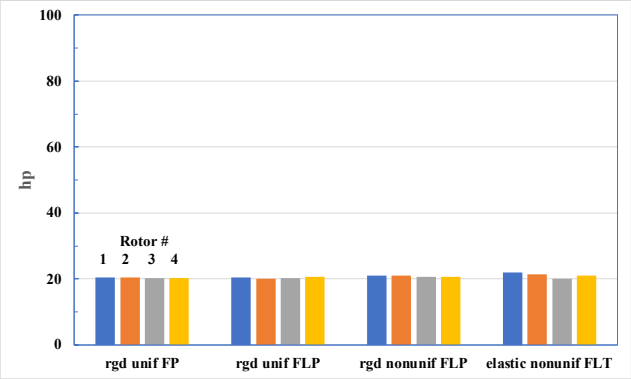

Figure 8g. Induced power, flyover.

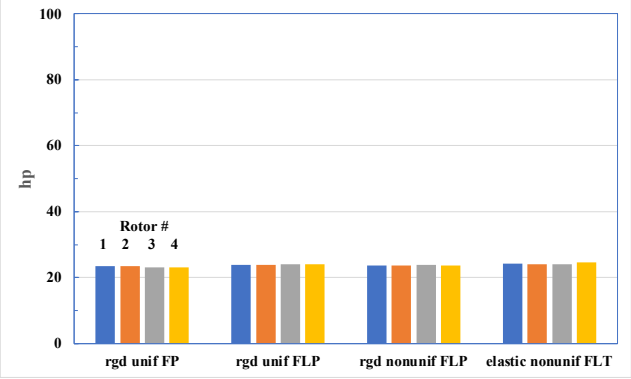

Figure 8h. Profile power, flyover.

Vertical blade loading, flyover. Figures 9a and 9b show loadz for all four rotors for blade models 1 and 4, respectively. There is longitudinal symmetry for blade model 1, but only rough longitudinal symmetry for blade model 4. The lack of symmetry for blade model 4 is attributed to slight differences in the trim collective and thrust of the individual rotors, Figs. 8c-8d. Figures 10a-10b and 11a-11b show comparisons of loadz for the four blade models; two blade models are considered in each figure. Lastly, Figs. 12a-12b shows loadz for blade models 1 and 4, left and right rotor pairs. Figures 12a-12b show the loadz variations of Ref. 2 (blade model 1) and for blade model 4. Reference 2 showed the rigid blade prediction for the front right rotor (Fig. 4d, Ref. 2), which is the same as the blue dashed-dotted line in Fig. 12b. Figures 11a-11b and 12a-12b show that blade elasticity has a significant effect on the vertical blade loading in flyover.

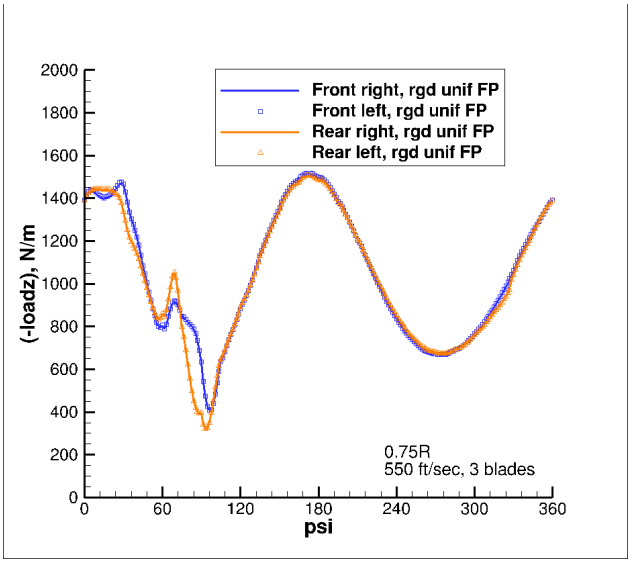

Figure 9a. 0.75R, rigid uniform FP (blade model 1), all four rotors, flyover.

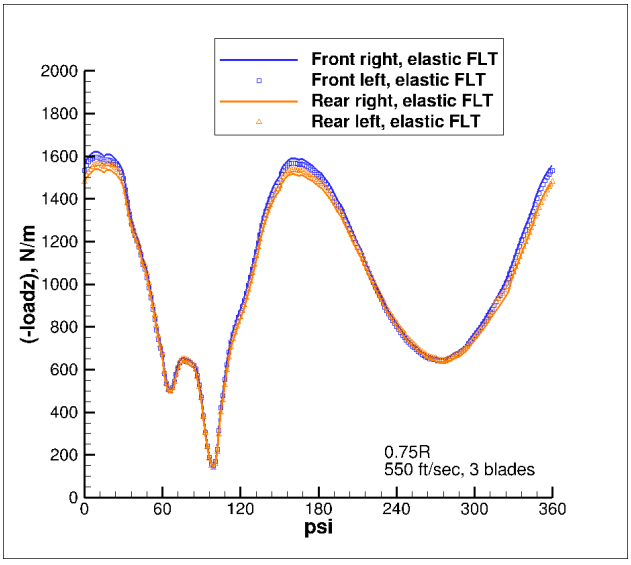

Figure 9b. 0.75R, elastic nonuniform FLT (blade model 4), all 4 rotors, flyover

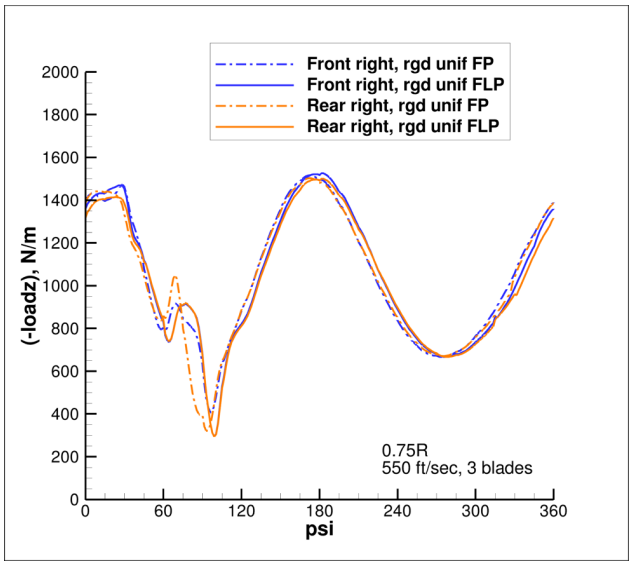

Figure 10a. 0.75R, rigid uniform FP and FLP (blade models 1 and 2), flyover.

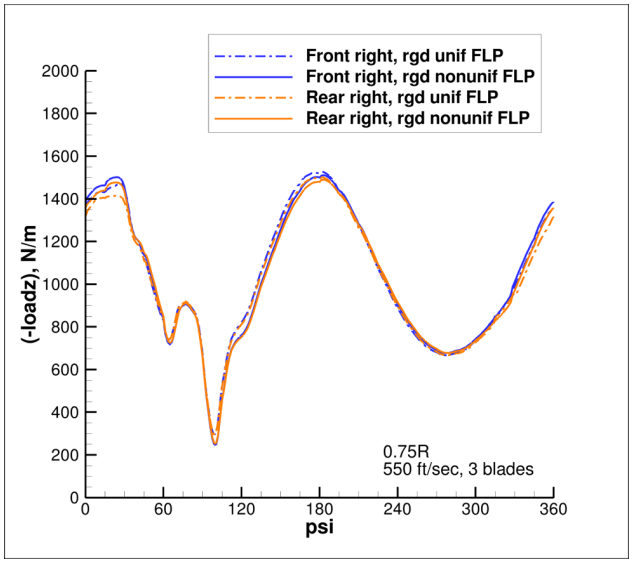

Figure 10b. 0.75R, rigid uniform and nonuniform FLP (blade models 2 and 3), flyover.

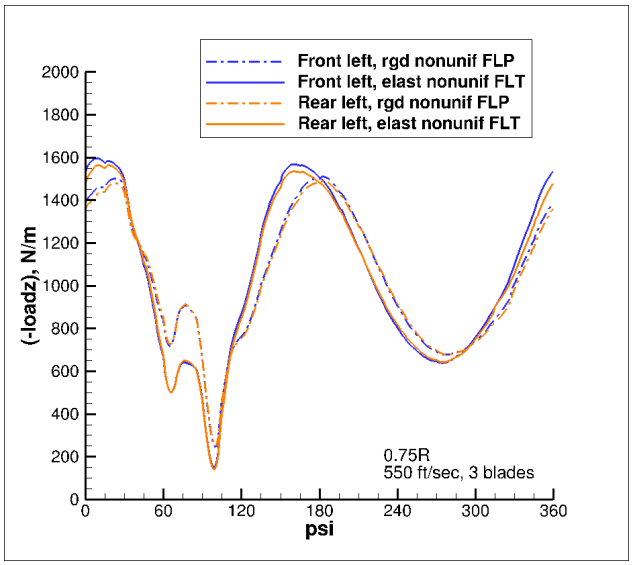

Figure 11a. Rigid nonuniform FLP and elastic nonuniform FLT (blade models 3 and 4), left rotors, flyover.

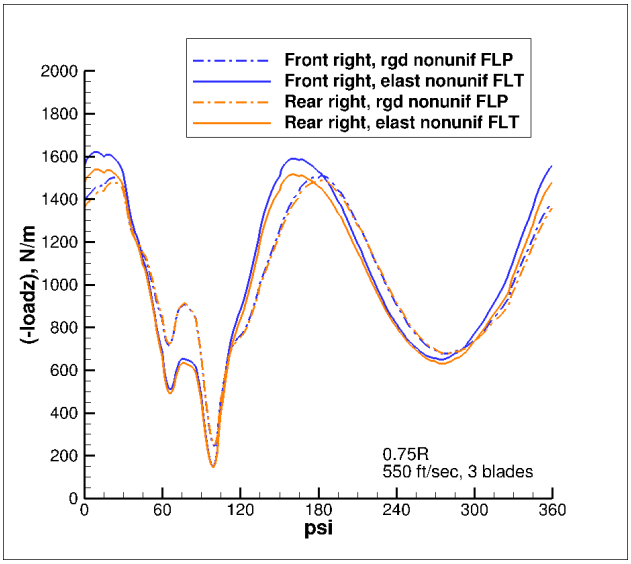

Figure 11b. Rigid nonuniform FLP and elastic nonuniform FLT (blade models 3 and 4), right rotors, flyover.

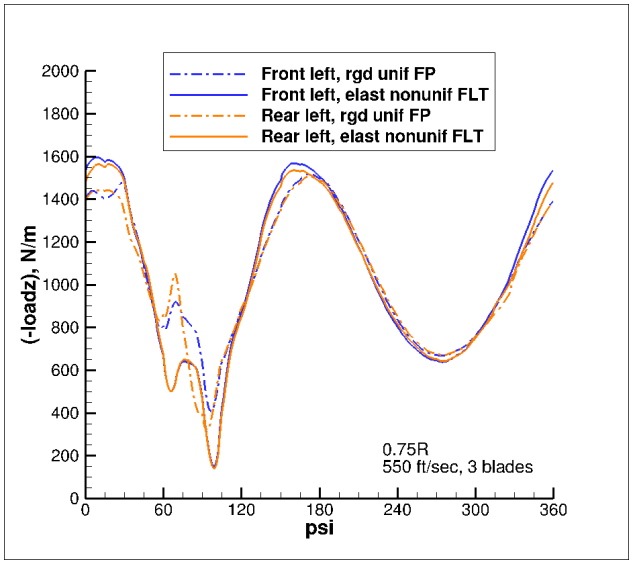

Figure 12a. Rigid uniform FP and elastic nonuniform FLT (blade models 1 and 4), left rotors, flyover.

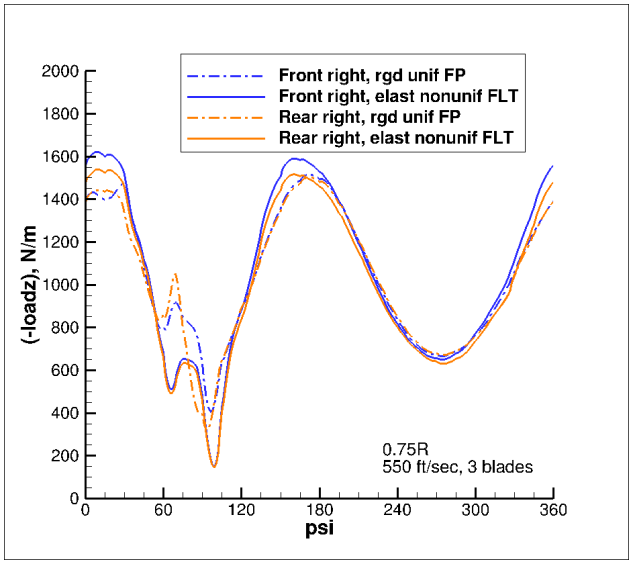

Figure 12b. Rigid uniform FP and elastic nonuniform FLT (blade models 1 and 4) right rotors, flyover.

Quadrotor noise, flyover. Figure 13 shows the noise results. The following observations can be made:

a) For all blade models, only the loading noise is different – the thickness and broadband self noise are almost the same for all four models. Thus, the trend for the total noise follows the trend for the loading noise.

b) The addition of the lag hinge to the rigid blade with uniform properties increases the loading noise by ~3 dBA (blade models 1 and 2).

c) For the rigid nonuniform blade, a ~1 dBA reduction in loading noise is obtained (blade models 2 and 3).

d) Results for blade models 3 and 4 do not show any significant difference in the loading noise levels (74 dBA). As discussed in the Approach section, preliminary reasons for this insensitivity to elasticity are the high blade torsional stiffness and the small blade radius. This result needs to be confirmed through further analysis with current and other blade designs and additional operating conditions.

e) EPNL changes by approximately 2 to 3 EPNdB between the blade models, unlike in approach where it is insensitive to the blade models.

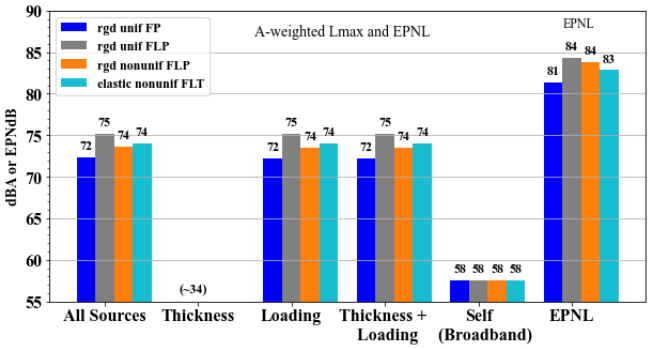

Figure 13. Quadrotor noise sources (all four rotors), blade models 1-4, flyover.

Takeoff

Quadrotor trim and performance, takeoff. Results for takeoff (~55 kts) are shown in Figs. 14a-14h. Figure 14f shows that the interference power in takeoff is very small; this is like in flyover and unlike in approach (approach involves relatively large interference power).

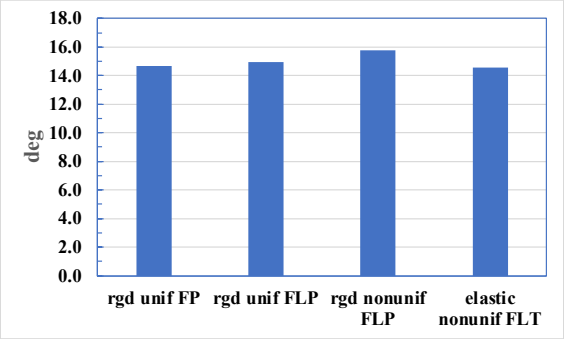

Figure 14a. Collective, average, takeoff.

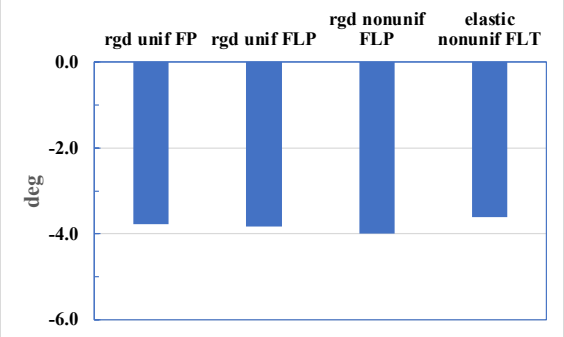

Figure 14b. Quadrotor pitch, takeoff.

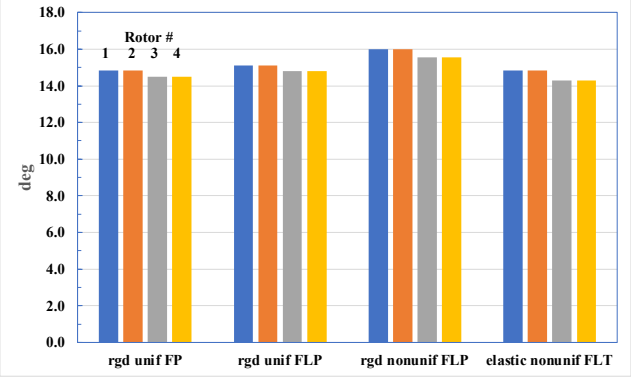

Figure 14c. Collective, rotors 1-4, takeoff.

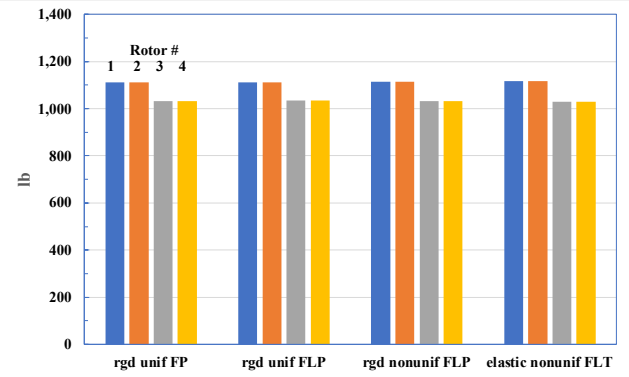

Figure 14d. Thrust, rotors 1-4, takeoff.

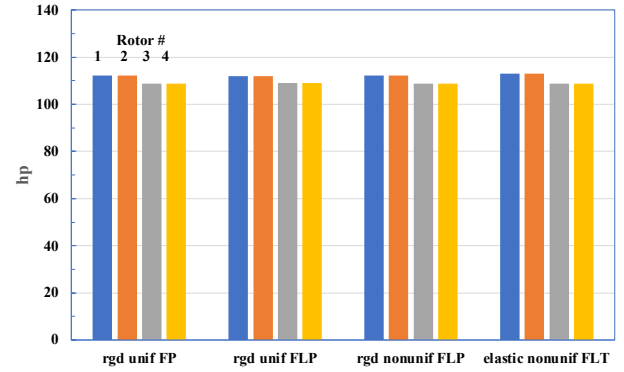

Figure 14e. Total power, takeoff.

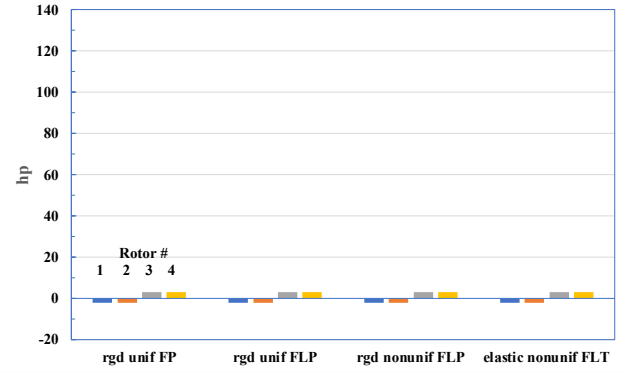

Figure 14f. Interference power, takeoff.

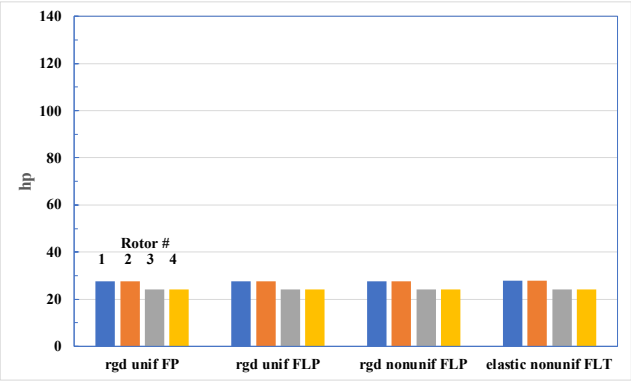

Figure 14g. Induced power, takeoff.

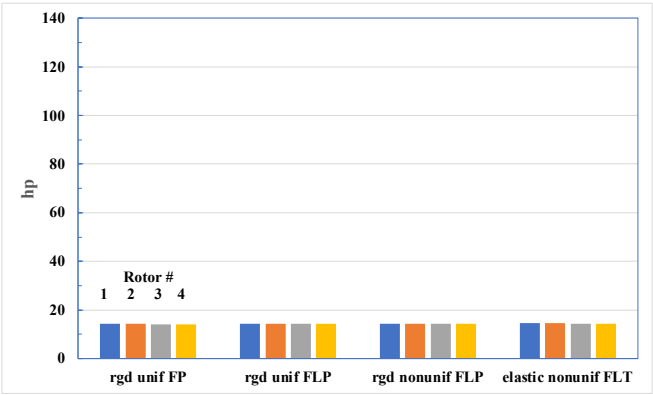

Figure 14h. Profile power, takeoff.

Vertical blade loading, takeoff. Figure 15 shows the vertical blade loading for all four rotors for blade model 1. There is longitudinal symmetry – the front left and right rotors behave very similarly; the same holds for the rear rotor pair. In the following figures, results for only the right-side rotor pair (front and rear right) are shown. Figures 16a-16c show comparisons of loadz for the four blade models; two blade models are considered in each figure. Lastly, Fig. 17 shows loadz for blade models 1 and 4. Reference 2 showed the rigid blade prediction for the front right rotor (Fig. 4d, Ref. 2), which is the same as the blue dashed-dotted line in Fig. 17. Figures 16c and 17 show that blade elasticity has a noticeable effect on the vertical blade loading.

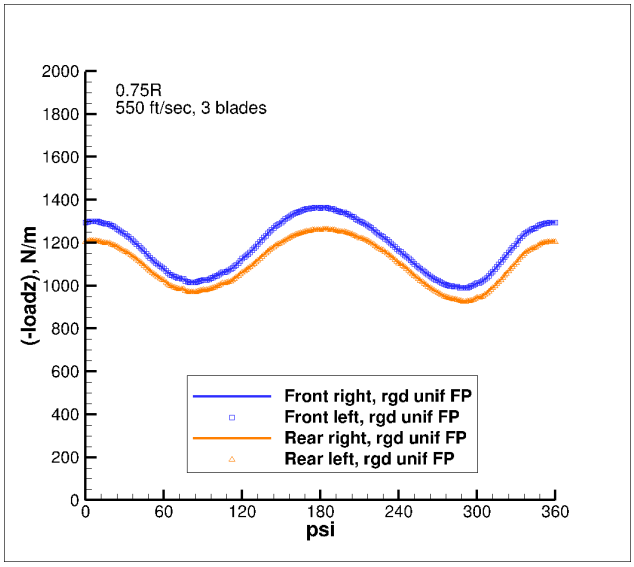

Figure 15. 0.75R, rigid uniform FP (blade model 1), all four rotors, takeoff.

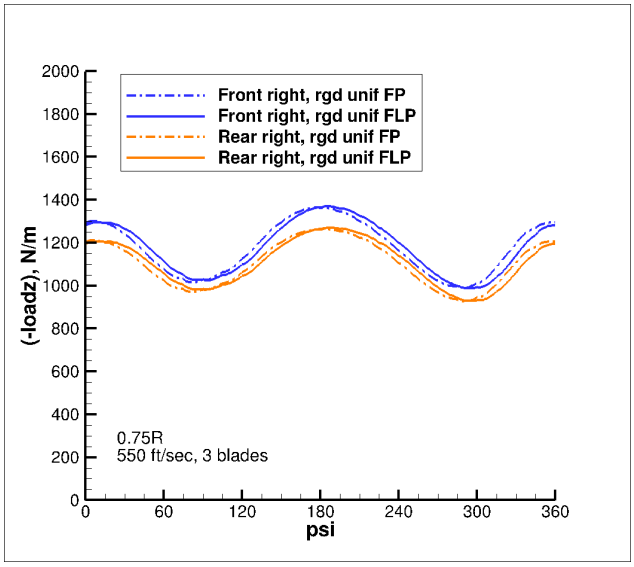

Figure 16a. 0.75R, rigid uniform FP and FLP (blade models 1 and 2), takeoff.

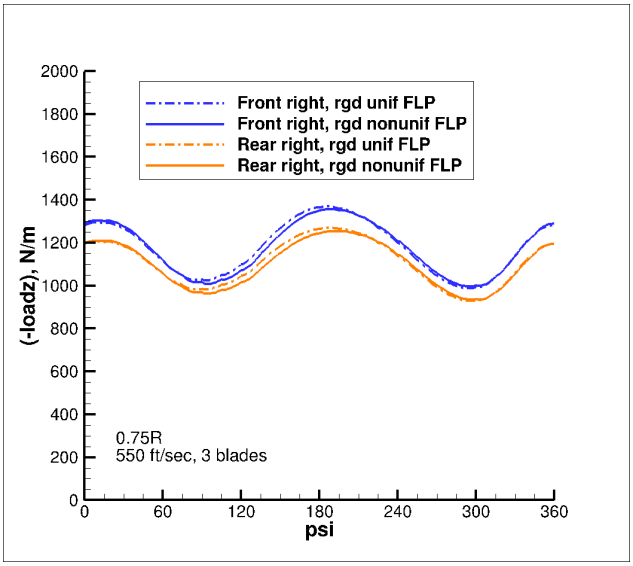

Figure 16b. 0.75R, rigid uniform and nonuniform FLP (blade models 2 and 3), takeoff.

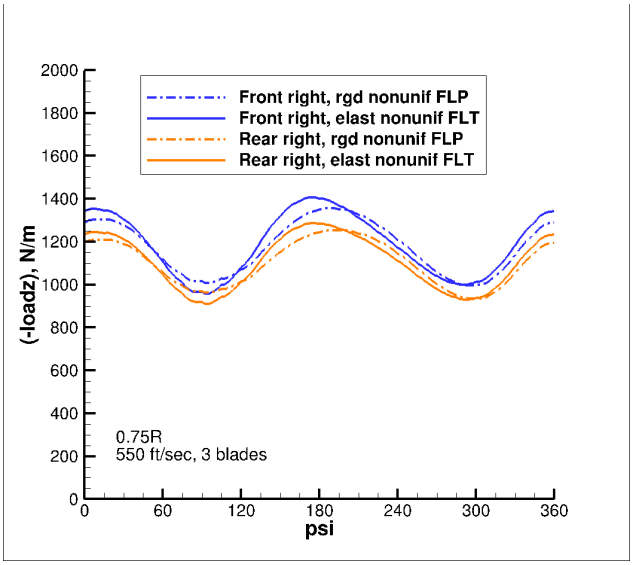

Figure 16c. 0.75R, rigid nonuniform FLP and elastic nonuniform FLT (blade models 3 and 4), takeoff.

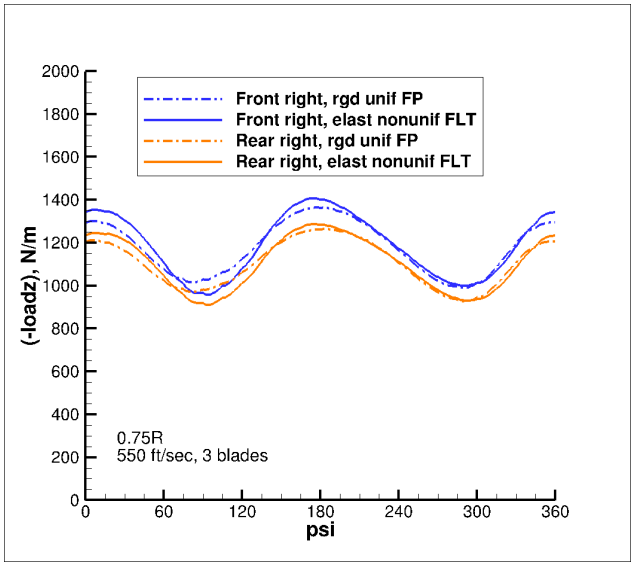

Figure 17. 0.75R, rigid uniform FP and elastic nonuniform FLT (blade models 1 and 4), takeoff.

Quadrotor noise, takeoff. Figure 18 shows the noise results. In contrast to approach and flyover, takeoff noise levels are insensitive to the blade models. For all four blade models, the broadband (self) noise is the primary contributor (53-54 dBA) to the total noise (56 dBA). The loading noise (51-52 dBA) is smaller than the broadband noise. EPNL is the same for all blade models.

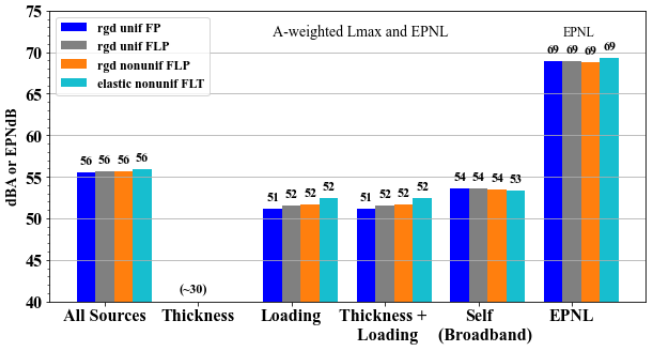

Figure 18. Quadrotor noise sources (all four rotors), blade models 1-4, takeoff.

Summary results – approach, flyover, takeoff

Noise results for all three flight conditions are summarized in this section. Also, potential follow-on work is discussed.

Noise, three flight conditions. The rigid uniform flap-pitch predictions of Ref. 2 (original blade model) and the current elastic nonuniform flap-lag-torsion predictions, blade models 1 and 4 respectively, are compared These two blade models are different in three ways: 1) no lag hinge vs. with lag hinge, 2) uniform spanwise properties vs. nonuniform spanwise properties, and 3) rigid vs. elastic blades. The previous sections showed that, qualitatively, the trim parameters and vertical blade loading are noticeably different for blade models 1 and 4 (especially, the 0.75R time histories, Figs. 6,

12, and 17). For noise, almost all the differences (deltas) in noise magnitude between these results are due to the addition of the lag hinge and the introduction of nonuniformities. The quadrotor with rigid nonuniform flap-lag-pitch blades (model 3) and that with elastic nonuniform flap-lag-torsion blades (model 4) do not produce noticeably different noise levels (Figs. 7, 13, and 18). As discussed in the Approach section, preliminary reasons for this insensitivity to blade elasticity are the high blade torsional stiffness and the small blade radius of 550/3.

Figures 19a-19c show noise results for the quadrotor in approach, flyover, and takeoff. Results for blade models 1 and 4 are shown in Figs. 19a-19b, respectively. The Fig. 19a results are the same as shown earlier (Fig. 4e of Ref. 2); Fig. 19b shows the current results.

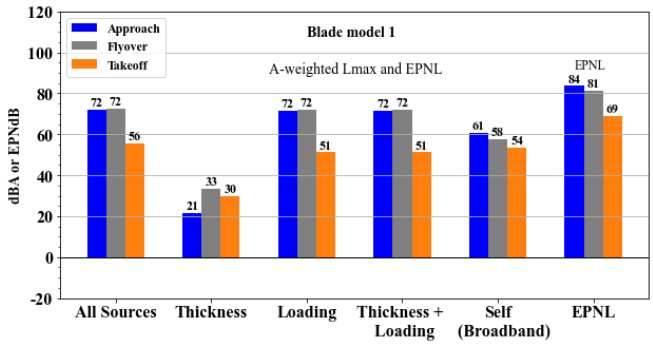

Figure 19a. Quadrotor noise sources (all four rotors), three conditions, blade model 1 (earlier results, Fig. 4e, Ref. 2).

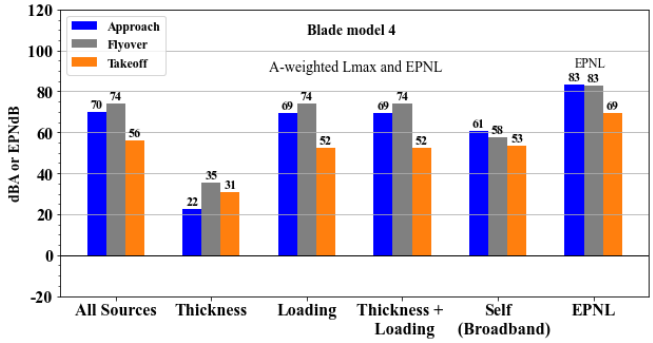

Figure 19b. Quadrotor noise sources (all four rotors), three conditions, blade model 4.

Figure 19c shows the difference in noise, delta, between the results of Figs. 19b and 19a – that is, the delta in quadrotor noise between the blade models 4 and 1 ("ending point vs. starting point"). A significant difference (around 2 dBA) in the quadrotor loading noise is seen in Fig. 19c.

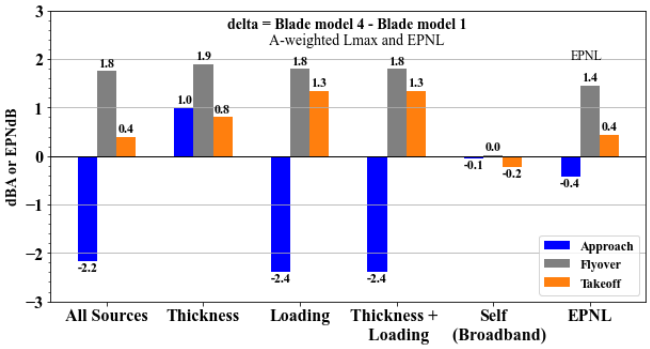

Figure 19c. delta: blade-model-4-noise minus blade-model-1-noise, all four rotors, three conditions.

Follow-on work. The possibility of follow-on work is discussed as follows. Potential topics for research on blade optimization to reduce noise are:

1. Since the current 550/3 blade has high torsional stiffness, a parametric study involving the torsion frequency could be conducted; lowering the torsion frequency may introduce larger elastic effects on quadrotor acoustics and reduce vehicle weight, hopefully in a beneficial manner. The parametric study would involve a redesign of the blade.
2. The present linear taper and twist distributions could be optimized with the goal of better acoustics. This calls for a blade redesign. The objective here should be to obtain benefits across all flight regimes. The present taper/twist distribution reduces approach noise but increases flyover noise (Fig. 19c). Approach and flyover will benefit first from loading and thickness noise reductions, while takeoff will first benefit from self-noise reduction.
3. Blade tip geometry is another parameter that can be optimized to get better acoustics. This calls for a blade redesign. Reference 15 has shown the acoustic benefit of tip dihedral, tip chord, and tip sweep for the Airbus AS350 SD vehicle. Reference 16 shows the acoustic benefit of tip dihedral (droop) for a conceptual single main rotor vehicle.
4. References 17 and 18 contain several concepts and technologies for noise reduction and these could be studied for potential follow-on work.

Contributions of front and rear rotor pairs

The contributions of the front and rear rotors to noise (A-weighted Lmax, EPNL, and OASPL) are presented in this section. Results for blade models 1 and 4 are given for all three flight conditions. A table summarizing the results of this study is included at the end.

Figure 20a-20f show the results in approach for blade models 1and 4; noise sources for the front and rear rotors and for all four rotors are shown. Figures 20a-20b show that the rear

rotors contribute more than the front rotors to the loading noise (and EPNL). Thickness and self (broadband) noise are roughly the same for the front and rear rotors (both blade models). In Figs. 20a-20b, the "All 4 rotors on" results are the same as the approach results in Figs. 19a-19b.

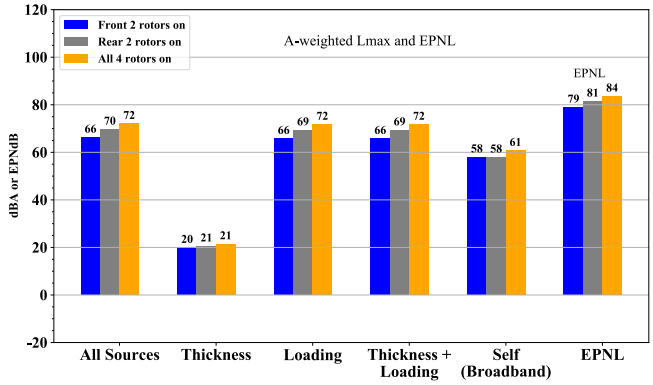

Figure 20a. Rigid uniform FP blades (model 1) – front and rear rotors, approach.

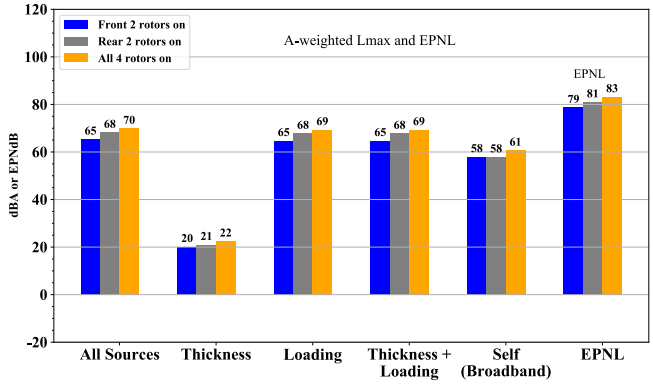

Figure 20b. Elastic nonuniform FLT blades (model 4) – front and rear rotors, approach.

Figures 20c-20d show the total approach OASPL and Figs. 20e-20f show the thickness and loading (t+l) and the broadband (bb) self noise contributions to OASPL. Compared to the front rotors, the larger contribution of the rear rotors to the total noise can be seen in Figs. 20c-20d (consistent with Figs. 20a-20b). Also, the front rotors' peak total OASPL occurs roughly a couple of seconds earlier than the corresponding peak for the rear rotors (Figs. 20c-20d). Figures 20e-20f show the larger contribution of the rear rotors to the t+l noise. Also, the broadband noise is roughly the same for the front and rear rotors. These trends are consistent with Figs. 20a-20b. The front rotors' t+l noise peak occurs earlier than that of the rear rotors by a couple of seconds (Figs. 20e-20f).

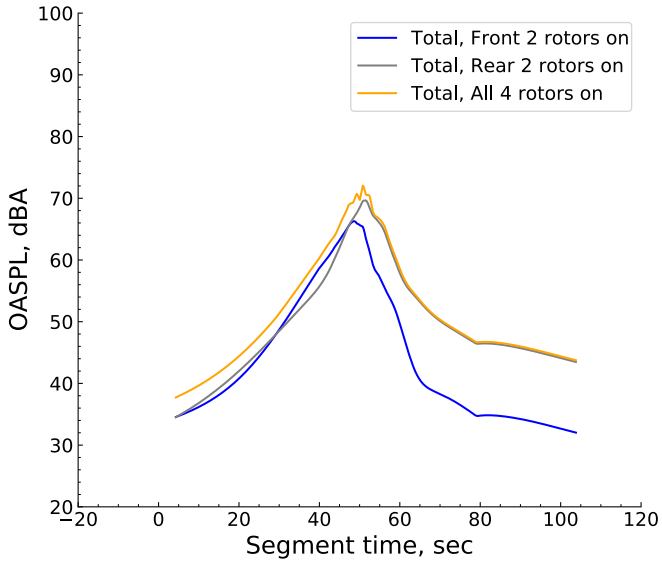

Figure 20c. Total OASPL – rigid uniform FP blades (model 1), approach.

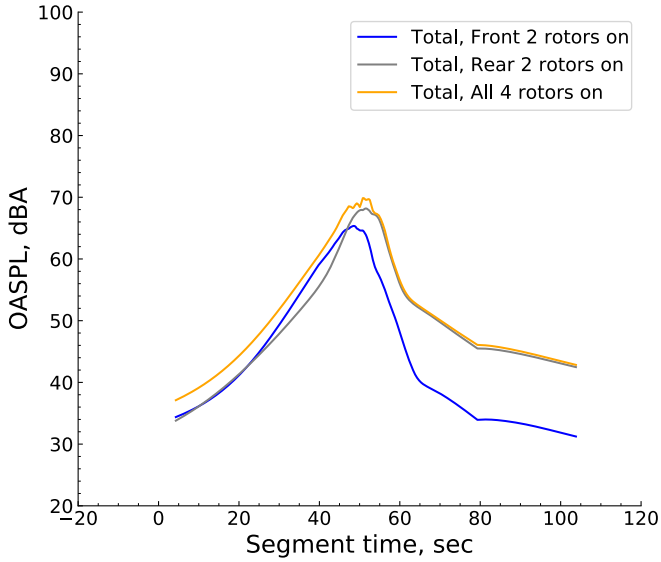

Figure 20d. Total OASPL – elastic nonuniform FLT blades (model 4), approach.

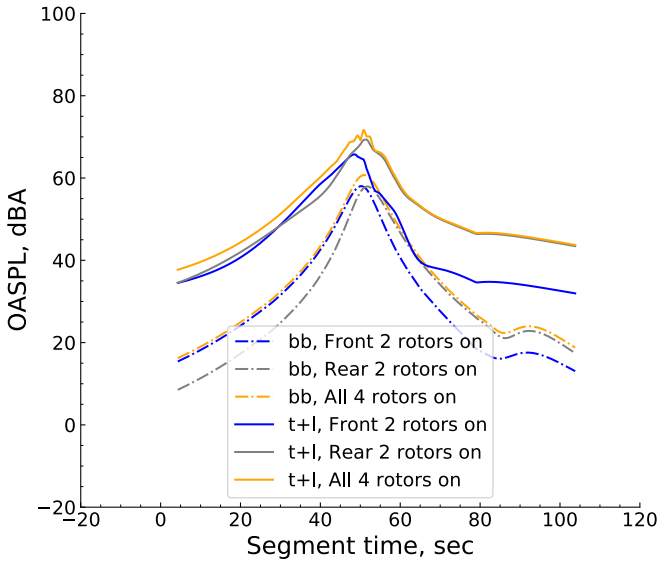

Figure 20e. OASPL, thickness-and-loading and broadband (self) – rigid uniform FP blades (model 1), approach.

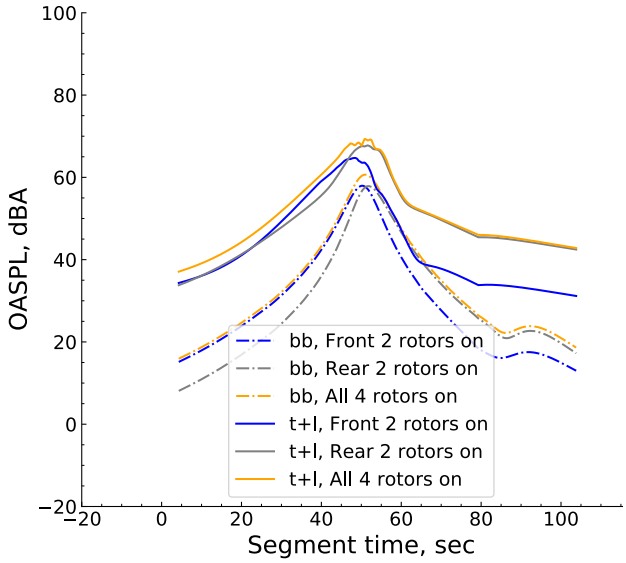

Figure 20f. OASPL, thickness-and-loading and broadband (self) – elastic nonuniform FLT blades (model 4), approach.

Figures 21a-21f show results for the flyover condition. Figures 21a-21b show a trend reversal – the rear rotors contribute less than the front rotors to the loading noise for the rigid model, and the opposite is true for the elastic model where the rear rotors contribute more than the front rotors. For the thickness noise and EPNL, however, the rear rotors contribute more, for both blade models. The self (broadband) noise is roughly the same for the front and rear rotors (both blade models). In Figs. 21a-21b, the "All 4 rotors on" results are the same as the flyover results in Figs. 19a-19b.

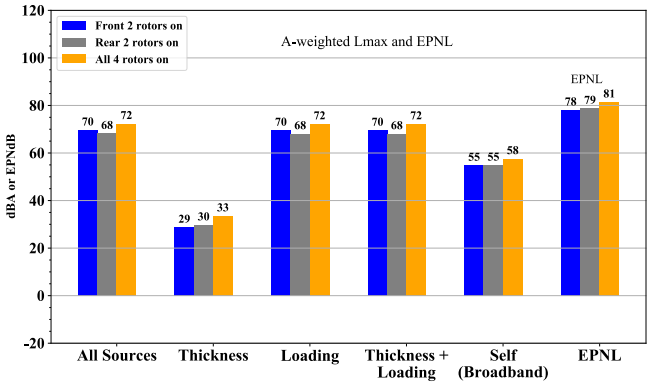

Figure 21a. Rigid uniform FP blades (model 1) – front and rear rotors, flyover.

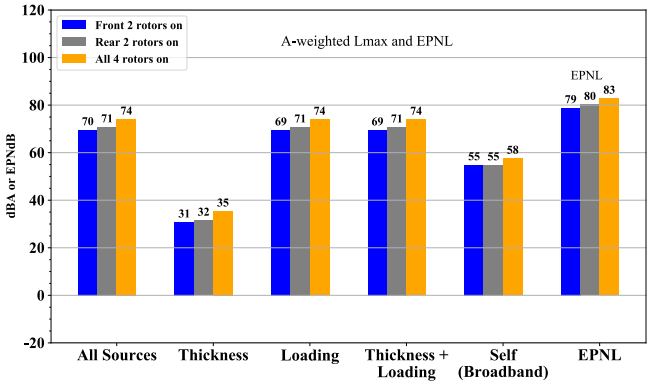

Figure 21b. Elastic nonuniform FLT blades (model 4) – front and rear rotors, flyover.

Figures 21c-21d show the total flyover OASPL and Figs. 21e-21f show the t+l and bb noise contributions to OASPL. The blade-model-related trend reversal seen in Figs. 21a-21b can also be seen in Figs. 21c-21f. The front rotors' peak total OASPL occurs slightly before the corresponding peak for the rear rotors; the same holds for the t+l noise peak. The bb noise is roughly the same for the front and rear rotors.

Figures 22a-22f show results for takeoff. In takeoff, self (broadband) noise is more important than in approach and flyover, and the overall trends are strongly dependent on the broadband noise component. Figures 22a-22b show that the front rotors contribute more than the rear rotors to the total and broadband noise. Because the broadband component has a larger magnitude, it determines the overall trend. In Figs.

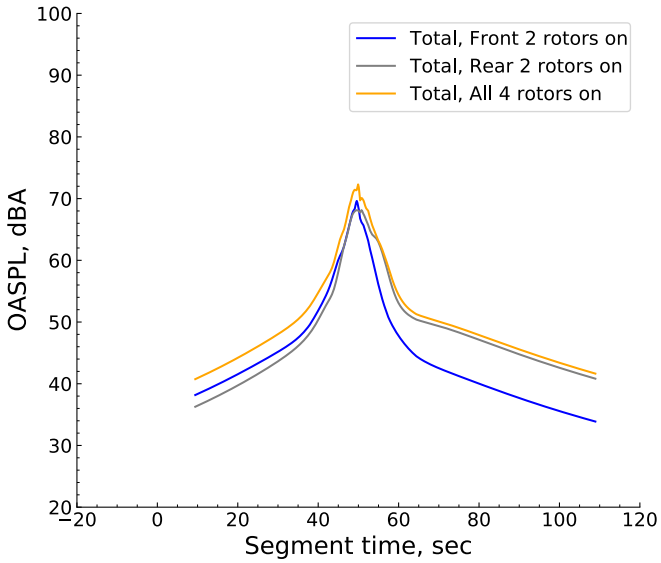

Figure 21c. Total OASPL – rigid uniform FP blades (model 1), flyover.

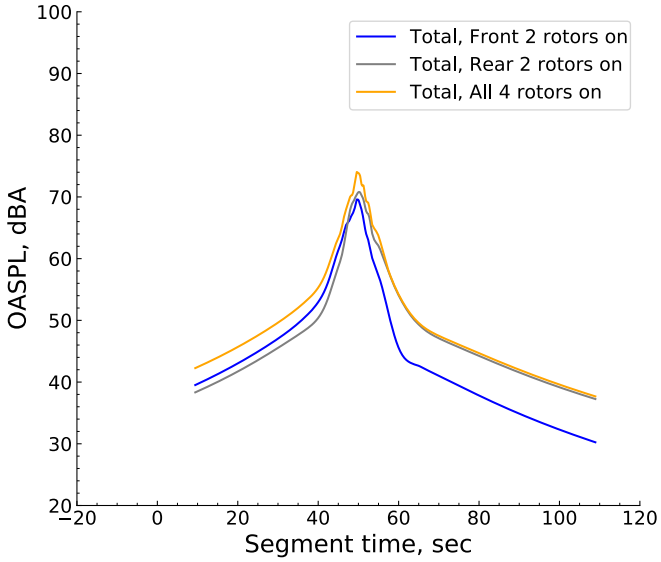

Figure 21d. Total OASPL – elastic nonuniform FLT blades (model 4), flyover.

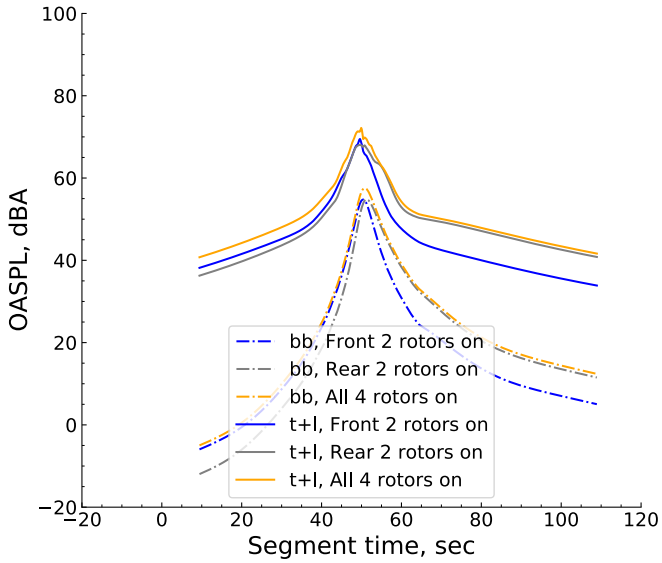

Figure 21e. OASPL, thickness-and-loading and broadband (self) – rigid uniform FP blades (model 1), flyover.

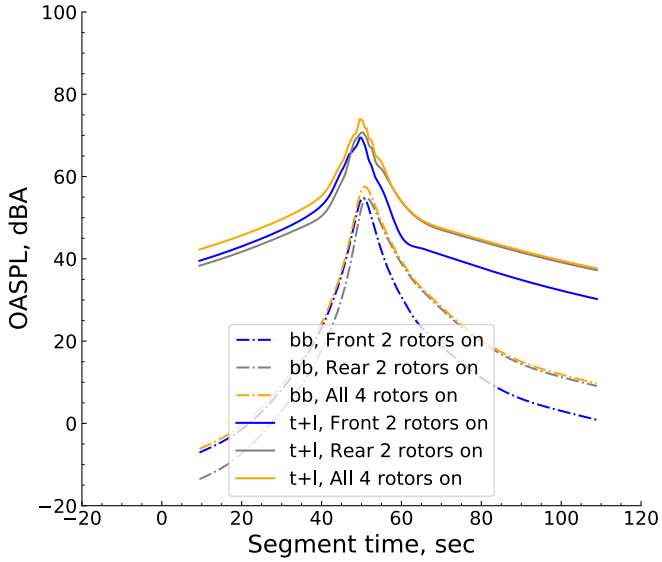

Figure 21f. OASPL, thickness-and-loading and broadband (self) – elastic nonuniform FLT blades (model 4), flyover.

22a-22b, the "All 4 rotors on" results are the same as the takeoff results in Figs. 19a-19b.

Compared to the rear rotors, the larger contribution of the front rotors to the total flyover OASPL can be seen in Figs. 22c-22d. Also, the front rotors' peak total OASPL occurs slightly earlier than the corresponding peak for the rear rotors. Figures 22e-22f show that the bb contribution is larger than the t+l contribution for both blade models, and the front rotors' bb contribution is larger than the rear rotors' bb contribution. This bb trend determines the trends seen in Figs.

22a-22f, i.e., the front rotors contribute more than the rear rotors to the total noise.

Table 3 (placed after the last section of the paper) summarizes the results for approach, flyover, and takeoff.

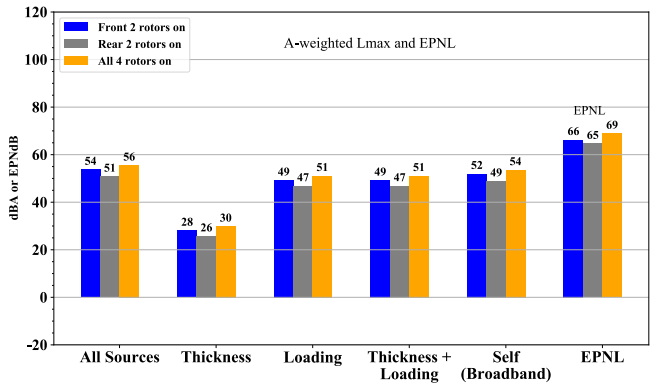

Figure 22a. Rigid uniform FP blades (model 1) – front and rear rotors, takeoff.

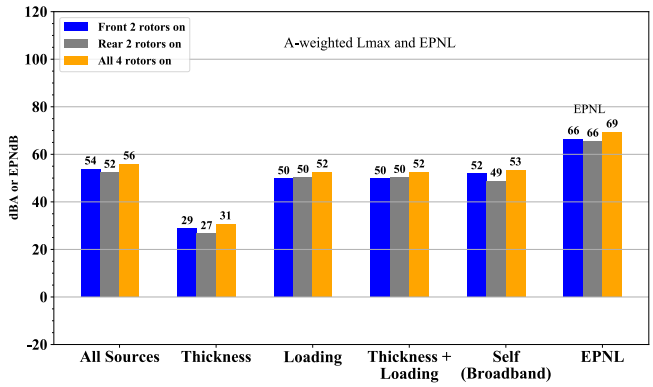

Figure 22b. Elastic nonuniform FLT blades (model 4) – front and rear rotors, takeoff.

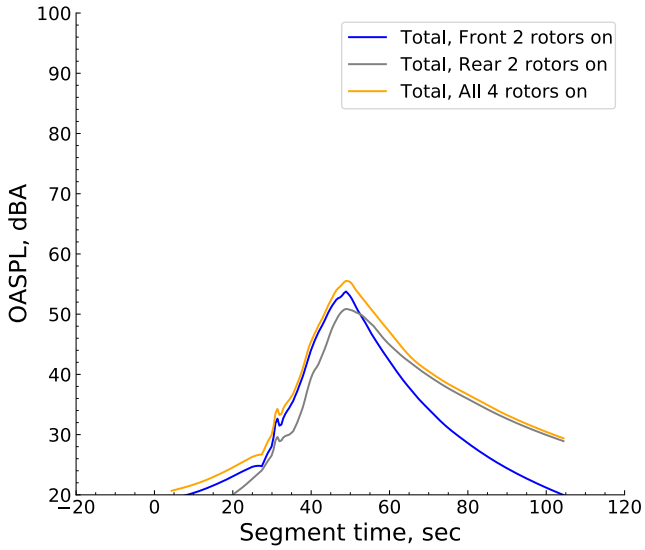

Figure 22c. Total OASPL – rigid uniform FP blades (model 1), takeoff.

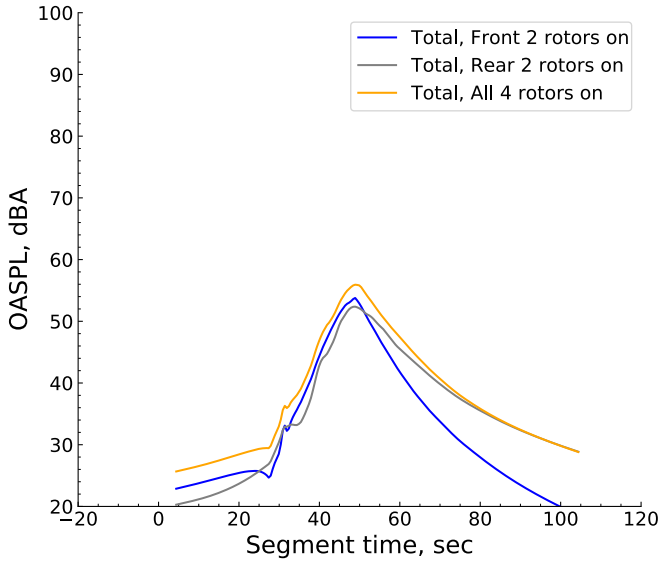

Figure 22d. Total OASPL – elastic nonuniform FLT blades (model 4), takeoff.

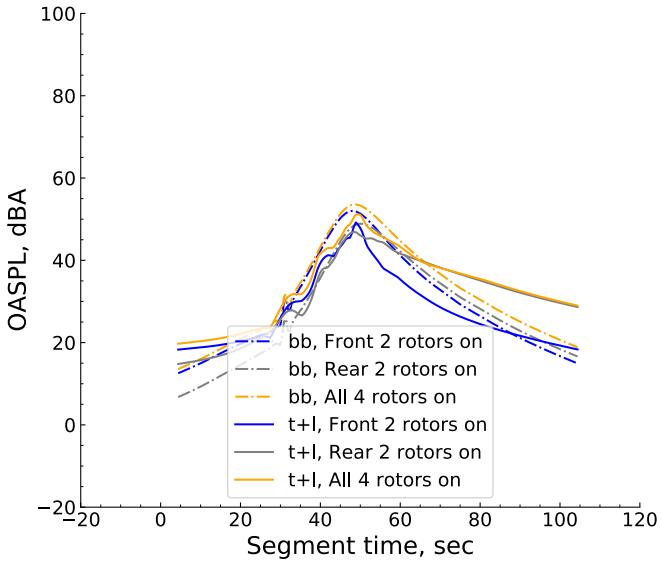

Figure 22e. OASPL, thickness-and-loading and broadband (self) – rigid uniform FP blades (model 1), takeoff.

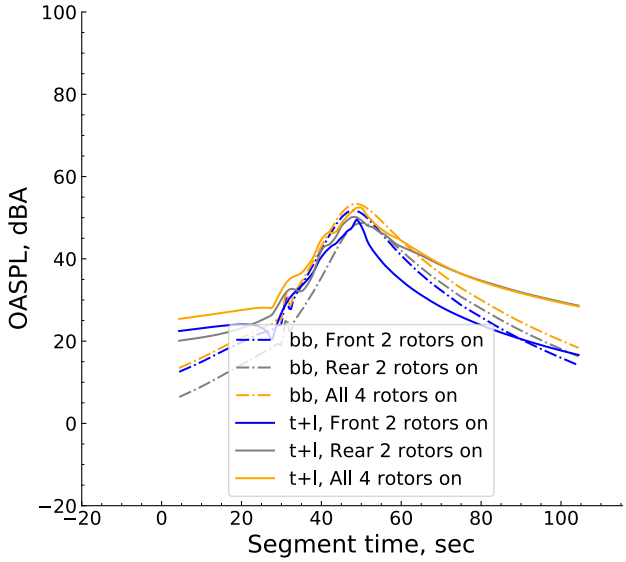

Figure 22f. OASPL, thickness-and-loading and broadband (self) – elastic nonuniform FLT blades (model 4), takeoff.

CONCLUSIONS

A 6-passenger urban air mobility (UAM) quadrotor concept vehicle was considered for acoustic analysis. The concept vehicle was designed under the NASA Revolutionary Vertical Lift Technology (RVLT) Project. The tip speed is 550 ft/sec, with three blades per rotor (550/3). Quadrotor trim and performance, 0.75R vertical blade loading for all four rotors, and noise sources were analyzed. Also, contributions of the front and rear rotor pairs to noise were studied. The individual rotor noise sources (thickness, loading, and broadband) were studied. Noise comparison was done using the A-weighted Lmax single sound level, the duration-based effective perceived noise level (EPNL), and the A-weighted Overall Sound Pressure Level (OASPL).

In this paper, "uniform" refers to uniform (constant) spanwise inertial and stiffness properties and "nonuniform" refers to inertial and stiffness properties that vary with span. The original 550/3 blades were rigid, uniform spanwise, and with flap and pitch degrees of freedom. The blade model was updated in this study: a lag hinge was added, spanwise and cross-sectional nonuniformities were introduced, along with elastic properties. Four blade models were considered in this study: 1) the original model, rigid uniform flap-pitch; 2) rigid uniform flap-lag-pitch; 3) rigid nonuniform flap-lag-pitch; and 4) elastic nonuniform flap-lag-torsion. Predictions were made for three flight conditions (approach, flyover, and takeoff) using the four blade models. The RVLT Toolchain was exercised using CAMRAD II and pyaaron/AARON/ANOPP2.

Specific conclusions are as follows:

1. Trim and performance: noticeable differences in the collective pitch were found for the four blade models. In approach, the interference power was relatively high compared to flyover and takeoff, with the rear rotors requiring more power than the front rotors. In flyover and takeoff, the interference power was very small.
2. Vertical blade loading: the azimuthal variations at 0.75R showed that blade elasticity resulted in noticeable differences in the vertical blade loading.
3. Noise sources: In approach and flyover, a 2 dBA loading noise difference (delta) was predicted between blade models 1 (rigid uniform flap-pitch) and 4 (elastic nonuniform flap-lag-torsion); the noise delta for takeoff was smaller, ~ 1 dBA. Most of the noise delta was due to the lag hinge and nonuniformities. This is consistent with the results of a 2022 study which had considered only approach; the current results extend this conclusion to flyover and takeoff also. The insensitivity of quadrotor noise to blade elasticity is currently attributed to the high blade torsional stiffness (frequency 6.41 per rev) and the small blade radius (9 ft) of the 550/3 design.
4. The contributions of the front and rear rotor pairs to noise were studied. Blade models 1 and 4 were considered. Specific findings include:
    a. Both blade models: in approach the rear rotors contribute more to the total noise and in takeoff, the front rotors contribute more.
    b. In flyover, for model 1, the front rotors contribute more; for model 4, the rear rotors contribute more.
    c. The loading noise is the primary contributor to the total noise in approach and flyover. In takeoff, the broadband (self) noise is the primary contributor. This was observed earlier in the 2022 study.

d. In approach, the front rotors' peak for total OASPL occurs earlier than that of the rear rotors. In flyover and takeoff, it occurs slightly early for the front rotors.

5. Suggestions for potential follow-on work on noise reduction include optimization of the blade geometry, especially tip geometry. The goal would be to reduce noise without worsening performance and loads.

Author contact:
Sesi Kottapalli sesi.b.kottapalli@nasa.gov
Christopher Silva christopher.silva@nasa.gov
Doug Boyd d.d.boyd@nasa.gov

ACKNOWLEDGMENTS

Insightful discussions with the following colleagues are gratefully acknowledged: Wayne Johnson, Larry Meyn, Gloria Yamauchi, and Bill Warmbrodt.

REFERENCES

1. Silva, C., and Johnson, W., "Practical Conceptual Design of Quieter Urban VTOL Aircraft," The Vertical Flight Society 77th Annual Forum Proceedings, Virtual, May 2021.
2. Kottapalli, S., and Silva, C., "Prediction of Quadrotor Acoustics Using RVLT Toolchain," VFS Aeromechanics for Advanced Vertical Flight Technical Meeting, San Jose, CA, January 2022.
3. Yamauchi, G., "A Summary of NASA Rotary Wing Research: Circa 2008–2018," NASA/TP 2019-220459, December 2019.
4. Johnson, W., "NDARC - NASA Design and Analysis of Rotorcraft: Theoretical Basis and Architecture," AHS Aeromechanics Specialists' Conference, San Francisco, CA, January 2010.
5. Hennes, C. C and Brentner, K. S, "The Effect of Blade Deformation on Rotorcraft Acoustics," 31st European Rotorcraft Forum, Florence, Italy, September 2005.
6. Derham, R. C, and Oh, B. K., "The Role of Blade Elasticity in the Prediction of Blade Vortex Interaction Noise," AHS/RAE International Specialists' Meeting on Rotorcraft Acoustics and Rotor Fluid Dynamics, Philadelphia, PA, October 1991.
7. Patt, D., Liu, L., and Friedmann, P. P., "Rotorcraft Vibration and Noise Prediction Using a Unified Aeroelastic Analysis," 44th AIAA/ASME/ASCE/AHS Structural Dynamics, and Materials Conference, Norfolk, VA, April 2003.
8. Liu, L., Patt, D., and Friedmann, P. P., "Active Vibration and Noise Reduction in Rotorcraft Using an Aeroelastic Simulation," AHS 4th Decennial Specialists' Conference in Aeromechanics, San Francisco, CA, January 2004.
9. Yin, J., van der Wall, B. G., and Wilke, G. A., "Rotor Aerodynamic and Noise Under Influence of Elastic Blade Motion and Different Fuselage Modeling," 40th European Rotorcraft Forum, Southampton, UK, September 2014.
10. Johnson, W., "CAMRAD II, Comprehensive Analytical Model of Rotorcraft Aerodynamics and Dynamics," Johnson Aeronautics, Palo Alto, CA, 1992-1999.
11. Meyn, L., "Rotorcraft Optimization Tools: Incorporating Rotorcraft Design Codes into Multi-Disciplinary Design, Analysis, and Optimization," AHS Technical Meeting on Aeromechanics Design for Vertical Lift, San Francisco, CA, January 2018.
12. Lopes, L., Burley, C., "Design of the Next Generation Aircraft Noise Prediction Program: ANOPP2," AIAA 2011-2854 17th AIAA/CEAS Aeroacoustics Conference, Portland, OR, June 2011.
13. Rohl, P.J., Dorman, P., Cesnik, C.E.S. and Kumar, D., "IXGEN—A Modeling Tool for the Preliminary Design of Composite Rotor Blades." American Helicopter Society Future Vertical Lift Aircraft Design Conference, San Francisco, CA, January 2012.
14. Palacios, R. and Cesnik, C. E. S., "Geometrically Nonlinear Theory of Composite Beams with Deformable Cross Sections," *AIAA Journal*, Vol. 46, No. 2, February 2008.
15. Boyd, D. D., Jr., "Midfidelity Rotorcraft Noise Optimization," Acoustics Technical Working Group Meeting, Hampton, VA, April 2018.
16. Johnson, W., "A Quiet Helicopter for Air Taxi Operations," VFS Aeromechanics for Advanced Vertical Flight Technical Meeting, San Jose, CA, January 2020.
17. Edwards, B., and Cox, C., "Revolutionary Concepts for Helicopter Noise Reduction - S.I.L.E.N.T. Program," NASA/CR-2002-211650, May 2002.
18. Rizzi, S. A, et al., "Urban Air Mobility Noise: Current Practice, Gaps, and Recommendations," NASA/TP–2020-5007433, October 2020.

Table 2. Approach, quadrotor noise (all four rotors) – blade models 1-4 (A-weighted Lmax and EPNL).

Noise source, dBA	1. rgd unif FP	2. rgd unif FLP	3. rgd nonunif FLP	4. elastic nonunif FLT
All	72.04	70.63	69.81	69.86
Thickness	21.45	21.89	21.87	22.44
Loading	**71.71**	**70.17**	**69.24**	**69.31**
Thickness + Loading	71.71	70.17	69.24	69.31
Self (Broadband)	60.72	60.72	60.69	60.66
Loading noise difference	**0.00**	**-1.54**	**-2.47**	**-2.40**
EPNL [EPNdB]	83.59	83.45	83.21	83.17

Table 3. Summary of contributions of front and rear rotor pairs, blade models 1 and 4.

Flight condition	Largest contributor to total noise	Primary noise source	Peak total OASPL occurrence
Approach	Rear	Loading	Front early
Flyover	Front[a] ; Rear[b]	Loading	Front slightly early
Takeoff	Front	Self (broadband)	Front slightly early

[a] Model 1; [b] Model 4